USGS
science for a changing world

In cooperation with U.S. Agency for International Development

Landsat ETM+ False-Color Image Mosaics of Afghanistan

By Philip A. Davis

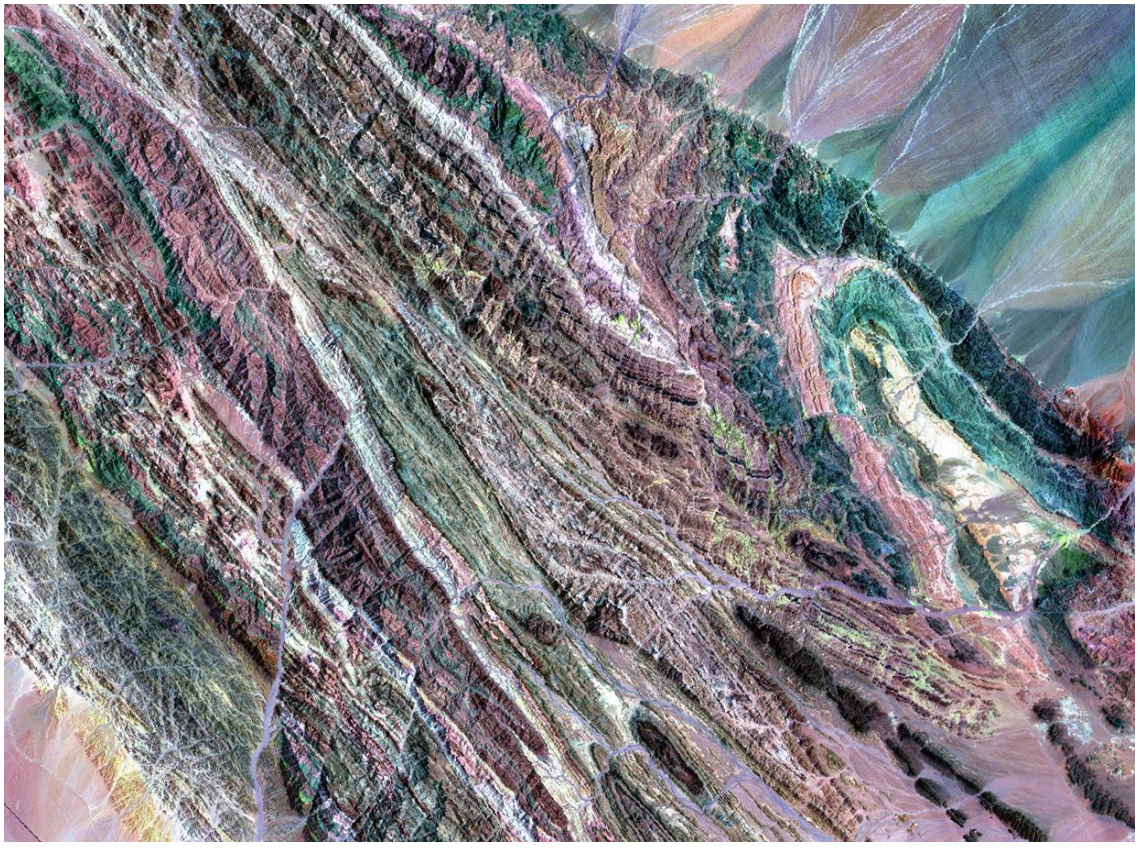

Open-File Report 2007-1029

U.S. Department of the Interior
U.S. Geological Survey

U.S. Department of the Interior
Dirk Kempthorne, Secretary

U.S. Geological Survey
Mark D. Myers, Director

U.S. Geological Survey, Reston, Virginia 20192
2007

For product and ordering information:
World Wide Web: http://www.usgs.gov/pubprod
Telephone: 1-888-ASK-USGS

For more information on the USGS—the Federal source for science about the Earth, its natural and living resources, natural hazards, and the environment:
World Wide Web: http://www.usgs.gov
Telephone: 1-888-ASK-USGS

Suggested citation:
Davis, P. A., 2007, Landsat ETM+ False-Color Image Mosaics of Afghanistan, U.S. Geological Survey Open-File Report 2007-1029, Washington, D.C., 22 p.

Any use of trade, product, or firm names is for descriptive purposes only and does not imply endorsement by the U.S. Government.

Contents

Introduction 5
Spectral Basis for False-Color Images 5
Processing of Landsat ETM+ to Produce False-Color Images 8
  Masking Vegetation, Snow/Ice, and Clouds 8
  Local-Area Histogram Stretch of Selected Landsat Band Images 9
  Reprojection of Landsat Map Tiles 9
References Cited 10

Figures

1. Landsat ETM+ natural-color image of an area in southeastern Afghanistan 11
2. Laboratory reflectance spectra for common iron-oxide minerals (Clark et al., 1993), resampled to the six Landsat ETM+ nonthermal bands, which are designated by "B" numbers 12
3. Laboratory reflectance spectra for minerals commonly found in sedimentary rocks and alluvium (Clark et al., 1993), resampled to the six Landsat ETM+ nonthermal bands, which are designated by "B" numbers 12
4. Laboratory reflectance spectra for common phyllosilicate minerals that occur in many different rock types and in alluvium (Clark et al., 1993), resampled to the six Landsat ETM+ nonthermal bands, which are designated by "B" numbers 13
5. Laboratory reflectance spectra for snow of different grain sizes and for average deciduous vegetation (Clark et al., 1993), resampled to the six Landsat ETM+ nonthermal bands, which are designated by "B" numbers. 13
6. Laboratory reflectance spectra for some common chemical and clastic sedimentary rocks (Clark et al., 1993), resampled to the six Landsat ETM+ nonthermal bands, which are designated by "B" numbers. 14
7. Laboratory reflectance spectra for different shales, which are fine-grained, fissile rocks (Clark et al., 1993), resampled to the six Landsat ETM+ nonthermal bands, which are designated by "B" numbers. 14
8. Laboratory reflectance spectra for common siliceous igneous rocks (Clark et al., 1993), resampled to the six Landsat ETM+ nonthermal bands, which are designated by "B" numbers. 15
9. Laboratory reflectance spectra for common mafic and ultramafic (anorthosite and dunite) igneous rocks (Clark et al., 1993), resampled to the six Landsat ETM+ nonthermal bands, which are designated by "B" numbers 15
10. Landsat ETM+ false-color image of same area shown in Figure 1 16
11. Russian geology (Sborshchikov et al., 1972) superposed on the Landsat ETM+ false-color image shown in Figure 10 17
12. Landsat ETM+ natural-color image of the northeastern border of the Registan Desert where drift sand (orange) meets bright white alluvium along a river valley 18
13. Landsat ETM+ false-color image of area shown in Figure 12 where drift sand (orange) meets alluvium (white and magenta), river (sinuous dark), and vegetation (green) 19

14. Landsat ETM+ natural-color image of an area north of Registan Desert in southern Afghanistan where irrigated alluvial areas are adjacent to desert pavement 20
15. Landsat ETM+ false-color image of area shown in Figure 14 where irrigated alluvial areas (green) are adjacent to desert pavement (dark brown) 21
16. Map tile scheme for the Afghanistan project (on a natural-color image base) with each 1^{o} x 2^{o} map quadrangle designated by its lower left corner latitude and longitude. 22

Landsat ETM+ False-Color Image Mosaics of Afghanistan

By Philip A. Davis[1]

Introduction

In 2005, the U.S. Agency for International Development and the U.S. Trade and Development Agency contracted with the U.S. Geological Survey to perform assessments of the natural resources within Afghanistan. The assessments concentrate on the resources that are related to the economic development of that country. Therefore, assessments were initiated in oil and gas, coal, mineral resources, water resources, and earthquake hazards. All of these assessments require geologic, structural, and topographic information throughout the country at a finer scale and better accuracy than that provided by the existing maps, which were published in the 1970's by the Russians and Germans. The very rugged terrain in Afghanistan, the large scale of these assessments, and the terrorist threat in Afghanistan indicated that the best approach to provide the preliminary assessments was to use remotely sensed, satellite image data, although this may also apply to subsequent phases of the assessments. Therefore, the first step in the assessment process was to produce satellite image mosaics of Afghanistan that would be useful for these assessments. This report discusses the production of the Landsat false-color image database produced for these assessments, which was produced from the calibrated Landsat ETM+ image mosaics described by Davis (2006).

Spectral Basis for False-Color Images

Much of Afghanistan has a semi-arid to arid climate. The climate, together with years of clear cutting vegetation for heating fuel, has produced the present-day landscape that is relatively barren, except in the far northeast corner of the country. The sparse vegetation cover and long history of folding, faulting, and erosion presents optimal conditions for using remotely sensed data to map exposed geologic materials and structure. The natural colors of semi-arid and arid environments, such as Afghanistan, are generally quite bland, consisting of subtle shades of brown, red, and yellow (Figure 1) that are produced mainly by the different amounts of iron-oxide minerals in exposed materials and by the different degrees of iron oxidation of these minerals that produce absorptions of sunlight at different wavelengths of the visible spectrum. The Landsat ETM+ sensor was developed as a space platform that could be used to map major mineral differences using selected short-wave infrared wavelength bands, as well as the visible and near-infrared wavelength bands that are collected by other, less sophisticated spaceborne sensors (e.g., IKONOS, Quickbird). Landsat ETM+ provides six nonthermal wavelength bands within the 0.4-2.5 micrometer wavelength range. Previous statistical studies have shown that color composite images using

[1] U.S. Geological Survey, 2255 North Gemini Drive, Flagstaff, AZ 86001

Landsat ETM+ bands 1 or 2, 3 or 4, and 5 or 7 provide the most geologic discrimination as three-band color composites (Chavez et al., 1982; Sheffield, 1985; Beauchemin and Fung, 2001). For this project, the three-band combination selected for the false-color image database was Landsat ETM+ bands 2, 4, and 7, displayed as blue, green, and red, respectively. Band 2 was used instead of band 1 because band 2 data were better tone matched in the low-contrast desert areas where local image enhancement accentuates very small image differences. The remainder of this section will discuss the geologic significance of the colors displayed in this false-color composite (FCC) database, as well as the chemical basis for the colors, which is extracted from the fundamental reflectance studies by Hunt and Salisbury (1970, 1971) and Hunt et al. (1971a, 1971b).

Iron is a minor element in many common minerals on Earth (and other planets of the inner Solar System). In some common minerals, such as magnetite, iron is a major element. Rocks having as little as a few weight percent magnetite are generally gray to black because magnetite (Fe_3O_4 or $FeO \cdot Fe_2O_3$) has both ferric (Fe^{+3}) and ferrous (Fe^{+2}) iron and each of these cations absorb light at several wavelengths in the visible and near-infrared wavelength regions, which results in magnetite's characteristic flat, low reflectance spectrum (Figure 2). Manganese has a similar spectrum and, in desert areas, rocks coated with manganese (known as desert varnish) are black regardless of the substrate. Iron-oxide is usually only a few weight percent of a rock's composition, but even this small amount can dramatically change the color of a rock. For example, sandstone generally has less than two weight percent iron oxide, but different degrees of iron oxidation can produce dramatic color variations ranging from brown, yellow, orange, to red.

Oxidation of ferrous iron produces ferric iron, which transforms FeO-bearing minerals (such as magnetite) into other iron-oxide minerals, such as hematite (Fe_2O_3 - red), goethite ($FeO \cdot OH$ – reddish and yellowish), and limonite ($FeO(OH) \cdot nH_2O$ – brown). Laboratory spectra of these minerals, which were convolved to the wavelength bands of Landsat ETM+ data, are shown in Figure 2. As FeO is oxidized to Fe_2O_3 to form hematite, the numerous absorptions of Fe^{+2} diminish and the major absorption of Fe^{+3} at 0.40 micrometers dominates the reflectance spectrum, which produces increasingly higher reflectance above the blue wavelength (centered at 0.45 micrometers). Hematite's higher reflectance in band 7 (displayed as red) relative to that in bands 2 and 4 produces red on the FCC image. Some sandstones and drift sand derived from sandstone, most basaltic pyroclastic cinders, and iron-ore deposits have bright red signatures on the FCC image. Hydrothermal systems and low-temperature hydration of iron-bearing minerals can produce goethite, which has an OH^- molecule that absorbs at 1.4 micrometers and secondarily at 1.9 micrometers. These absorptions produce a reflectance spectrum that is lower than that of hematite within the short-wave region (Figure 2). Complete hydration of iron-bearing minerals can produce limonite (common in soils), which has a water molecule that absorbs at 1.9 micrometers, which further reduces the reflectance within band 7 (Figure 2).

Quartz is a major mineral constituent in many sedimentary rocks and in certain igneous rocks. Igneous rocks also have various proportions of pyroxene and plagioclase, both of which have reflectance spectra similar to that of quartz (Figure 3). Therefore, rocks with these minerals that have not been weathered (which is rare) are generally white to gray in color. Calcite and dolomite are common carbonate (CO_3^{-2}) minerals in sedimentary rocks and alluvium derived from sedimentary rocks. The $CO_3^{=}$ molecule causes absorptions between 1.6 and 2.5 micrometers wavelength (within ETM+ bands 5 and 7) due to lattice vibrations (Hunt and Salisbury, 1971). Sulfate minerals also commonly occur in sedimentary and alluvial environments. The sulfate molecule does not produce absorptions within the short-wave region, but some common sulfate

minerals (such as gypsum and jarosite) contain OH^- and H_2O, respectively, which do produce absorptions in the short-wave region (Hunt and Salisbury, 1971b; Figure 3). Therefore, without significant amounts iron oxide, both of these mineral groups generally have high reflectance values in the visible (band 2) and near-infrared (band 4) wavelength regions and low reflectance in band 7 (Figure 3), thus producing FCC colors that are shades of blue. The much larger band-7 absorption in gypsum relative to carbonate minerals would suggest that these two mineral groups could be distinguished with Landsat data, but that is generally not the case. Jarosite, generally formed in ore deposits by oxidation of iron sulfide minerals, is an exception. In addition, there are some phyllosilicate minerals (kaolinite, montmorillonite; Figure 4) that also produce bluish FCC signatures, but these are generally more cyan than the dark blues produced by carbonates and sulfates. Water bound in these clay minerals produce H-O-H dipolar stretching and OH^- bending, whose overtones and combination tones cause absorptions within band 5 and band 7 (Hunt and Salisbury, 1970). Rocks containing muscovite or biotite, such as shale, are generally green on the FCC image, as a result of the depression of bands 1 and 7 reflectance relative to that of band 4. Rocks containing the phyllosilicates illite and chlorite are more difficult to distinguish because they should produce shades of red similar to that produced by iron oxides. Despite some of these mineral ambiguities, Landsat FCC images do allow mapping of geologic rock groups and provide wide-area coverage in relatively inaccessible terrain such as Afghanistan.

The reflectance spectra of rocks are generally more subdued than that of their mineral constituents, which produces ambiguities in rock identification using the six nonthermal Landsat band data. Figure 6 shows the reflectance spectra of some common clastic sedimentary rocks. The spectra for these rocks are depressed in the visible wavelength bands, relative to their major mineral constituent (quartz in the sandstones and calcite in the limestones), due to the presence of iron oxide. The reflectance spectra of shales (Figure 7) appear to be dominated by the reflectance of chlorite and illite clay minerals. The reflectance spectra of siliceous igneous rocks (Figure 8) are very similar to those of sandstones and siltstones (Figure 6), which make their discrimination very difficult using Landsat nonthermal image data, unless bedding can be seen in the imagery. A similar ambiguity exists with respect to mafic and ultramafic igneous rocks (Figure 9); most of the mafic igneous rocks have relatively flat spectra due to the presence of magnetite. However, ultramafic rocks are frequently altered because the surface environment is very different from their (deep) environment of formation. Thus, the reflectance spectrum of dunite (composed mostly of olivine – a high-temperature mineral) shows the Landsat-band absorptions (at bands 4 and 7) due to the conversion of olivine to hydrous clay minerals.

Figure 10 is a Landsat false-color image of an area near the southeastern border between Afghanistan and Pakistan. The area consists dominantly of sedimentary rock formations that have been intensely folded and faulted. This image shows much more geologic information than the natural-color image (Figure 1). The false-color image better depicts individual strata, allows regional correlations of strata, and better depicts structure, such as anticlines, synclines, and faults, compared to the natural-color image. When the Russians mapped Afghanistan in the early 1970's, the Landsat satellite did not exist. Thus, the most detailed Russian mapping (superposed on the Landsat false-color image in Figure 11) was very general. For example, the Russians mapped two sedimentary rock units in this area; one labeled Eo (Eocene) and the other labeled Ol (Oligocene). The Eocene unit is described as stratified clay, shale, siltstone, sandstone, limestone, marl, gypsum, and conglomerate. The Oligocene unit is described as stratified sandstone, siltstone, clay, conglomerate, limestone, marl, and siliceous and mafic volcanics. The units labeled with a Q are Late Quaternary and Recent detrital sediments. The colors shown in Figure 4 or 5 suggest that

there are sandstone units, either limestone, marl, or gypsum-rich units, and probably clay-rich layers throughout the area, but igneous rocks do not appear to exist in this particular area. Remote sensing data cannot determine the age of rocks; this may be inferred from stratigraphic position, if the age of at least one unit is known, but age differences can be very subtle, even in the field.

Processing of Landsat ETM+ to Produce False-Color Images

The false-color image database described in this report was produced from a three-band subset (ETM+ bands 2, 4, and 7) of the calibrated, six-band Landsat image data that were produced as 1º x 2º map tiles (Davis, 2006). Three steps were required to produce the false-color images, namely (1) the creation of digital masks for vegetation, snow and ice, and clouds; (2) the application of a local-area histogram stretch to selected Landsat bands; and (3) the transformation of the FCC images from Universal Transverse Mercator (UTM) to a geographic coordinate reference system.

Masking Vegetation, Snow/Ice, and Clouds

In order to preferentially enhance the geologic material within each map tile it was necessary to create image masks of vegetation, snow and ice, and clouds where they occur within any particular image map tile. The use of the different masks during image enhancement is discussed in the next section. The vegetation mask was constructed using a combination of three criteria applied to the six-band Landsat data, based on the general spectral characteristics of vegetation (Figure 5). The three criteria for vegetation consisted of the Normalized Difference Vegetation Index (NDVI), which is the ratio of (band 4-band 3)/(band 4 + band 3); the band 4/band 5 ratio; and the band 3*/band 3 ratio, where band 3* is the interpolated reflectance of bands 2 and 4 at wavelength of band 3. A picture element was classified as vegetation if its NDVI was greater than or equal to 0.325, its band 4/band 5 ratio was greater than 1.0, and its band 3*/band 3 ratio was greater than 1.0.

The logic required to accurately mask snow and ice was most difficult because the spectral characteristics of these two materials vary greatly within a map tile due to differences in grain size (shown in Figure 5), compaction, the snow/ice ratio, and the relative proportion of dust, sediment, or boulders to snow/ice on the surface of the ice flows. A picture element was classified as snow or ice if it satisfied one of four criteria: (1) the reflectance of band 5 was less than 1.3 percent of the reflectance sum of bands 1 through 4 and the reflectance sum of bands 1 through 4 was greater than 20 percent; (2) the reflectance of each of the first four bands was at least 10 percent and the band 4/band 5 reflectance ratio was greater than 3.0; (3) the reflectance of band 4 was at least 12 percent and the band 4/band 5 reflectance ratio was greater than 8.0; and (4) the reflectance of band 5 was greater than 12 percent, the reflectance of each of the first four bands was at least 16 percent, and the band 4/band 5 reflectance ratio was at least 1.7. These rules were developed by trial and error and visual inspection of the results; the rules were found to be as accurate as performing an unsupervised classification on the image data. The rules were designed to detect the lower limits of snow and ice, without including other geologic materials.

The development of a cloud mask was also difficult because of the gradation in opacity of the clouds toward their margins. Clouds were the smallest populated category of the three materials to be masked and, therefore, it was easier to construct the cloud masks using an unsupervised classifier on the six-band image data than it was to develop accurate spectral logic.

Each of the three masks were assigned a unique number and combined into a single image mask for use during the image enhancement step.

Local-Area Histogram Stretch of Selected Landsat Band Images

The algorithm used to locally stretch the image band data was developed by Pizer et al. (1987) and is referred to as adaptive histogram equalization. The picture-element area used to enhance the 28.5-m image data was 401 image rows x 401 image lines; the area used for the 14.25-m image data was twice those dimensions. The image band enhancement was performed on each of the three Landsat bands separately. The enhancement consisted of four steps. First, the entire image tile was locally enhanced and the enhanced image was stored in an image file and the vegetation and snow and ice picture elements were then removed from the original band image. Second, the remaining picture elements were locally enhanced and the cloud picture elements were then superposed onto the stored enhanced image file and then the cloud elements were removed from the original image. Third, the remaining picture elements were locally enhanced, and where these picture elements were adjacent to snow or ice, the enhanced value of each border picture element was averaged with its coincident picture element from the stored enhanced image. This averaging reduced sharp brightness discontinuities along geologic and snow/ice margins. The last step superposed the stored cloud, vegetation, and snow/ice picture elements onto the enhanced geologic image base produced in the third step. The results from this enhancement on bands 7, 4, and 2 were stored as a three-band image file, to be displayed as red, green, and blue, respectively. This procedure was performed on both the 28.5-m and 14.25-m Landsat image quads.

There are two situations where the false-color images have color inconsistencies. The first situation is along the border of the Registan Desert where drift sand adjacent to very bright alluvium (Figure 12) was stretched less than the drift-sand areas that are well within the desert. The bright alluvial borders increased the brightness range along the desert border, which caused the stretch on the drift sand to be less than that on the drift sand that is within the desert interior. This produced a yellow rim along the desert border (Figure 13). Attempts to isolate the bright alluvium and to stretch it and the drift sand separately produced more problems within the bright alluvium than the yellow color discontinuity. The second situation is where large vegetated areas (mostly irrigated fluvial valleys) are adjacent to old, darkened desert pavement (Figure 14). The vegetation mask algorithm did not remove the sparse vegetation and therefore vegetation picture elements, which have very low band 7 values (as shown in Figure 5), were included in the local histogram stretch of the adjacent desert pavement, which raised the pavement's band 7 (displayed in red) stretch values to produce magenta (Figure 15). Care was exercised in the vegetation masking process to not include geologic material. Within sparsely vegetated (shrub) alluvial areas, the distinction between vegetation and alluvium is not distinct and can change throughout large areas due to changes in vegetation species and alluvial substrate.

Reprojection of Landsat Map Tiles

Map tiles in UTM map projection provide very good local positional accuracy, but map tiles from adjacent UTM zones (Afghanistan has three zones) cannot be joined into a single image file unless the data are either reprojected to a common zone, which produces very poor positional accuracy within the other two zones, or reprojected to a geographic coordinate reference system. Reprojection of the UTM map tiles to a geographic reference system was performed according to the process described in Davis (2006), which used a second-order polynomial transformation and an x and y control-point grid of 90 x 90 (i.e., 8100 control points) for the 28.5-m map tiles. The

enhanced, 14.25-m map tiles required a 180 x 180 control-point grid. Once completed, each tile was trimmed to provide a 100 meter outside border in order to overlap adjacent map tiles. Each three-band enhanced map tile was then converted to an embedded geotiff image with a world file. The map tile geotiff and world file were compressed into a single digital file whose file name corresponds to the map tile number, image resolution, and projection. Therefore, each map tile has four compressed files.

All of the 28.5-m and 14.25-m map tiles containing the enhanced false-color Landsat images for Afghanistan can be downloaded from *http://gisdata.usgs.net/website/afghan*. An index map for the tile designations is shown in Figure 16.

References Cited

Beauchemin, M., and Fung, K. B., 2001, On statistical band selection for image visualization. Photogrammetric Engineering and Remote Sensing, v. 67, p. 571-574.

Chavez, P. S., Berlin, G. L., and Sowers, L. N., 1982, Statistical method for selecting Landsat MSS ratios. Journal of Applied Photographic Engineering, v. 8, p. 23-30.

Clark, R.N., Swayze, G. A., Gallagher, A. J., King, T. V. V., and Calvin, W. M., 1993, The U. S. Geological Survey, Digital Spectral Library: Version 1: 0.2 to 3.0 microns, U.S. Geological Survey Open File Report 93-592, 1340 p.

Davis, P. A., 2006, Calibrated Landsat ETM+ nonthermal-band image mosaics of Afghanistan. U.S. Geological Survey Open File Report 2006-1345, 18 p.

Doebrich, J. L., and Wahl, R. R., 2005, Geologic and Mineral Resource Map of Afghanistan, 1:850,000 scale, U.S. Geological Survey Administrative Report 2005.

Hunt, G., R., and Salisbury, J. W., 1970, Visible and near-infrared spectra of minerals and rocks: I. Silicate minerals. Modern Geology, v. 1, p. 283-300.

Hunt, G. R., and Salisbury, J. W., 1971, Visible and near-infrared spectra of minerals and rocks: II. Carbonates. Modern Geology, v. 2, p. 23-30.

Hunt, G. R., Salisbury, J. W., and Lenoff, C. J., 1971a, Visible and near-infrared spectra of minerals and rocks: III. Oxides and hydroxides. Modern Geology, v. 2, p. 195-205.

Hunt, G. R., Salisbury, J. W., and Lenoff, C. J., 1971b, Visible and near-infrared spectra of minerals and rocks: IV. Sulphides and sulphates. Modern Geology, v. 3, p. 1-14.

Pizer, S. M., Amburn, E. P., Austin, J. D., Cromartie, R., Geselowitz, A., Romeny, H., Zimmerman, B., and Zuiderveld, K., 1987, Adaptive histogram equalization and its variations. Computer Vision, Graphics and Image Processing, v. 39, p. 355-368.

Sheffield, C., 1985, Selecting band combinations from multispectral data. Photogrammetric Engineering and Remote Sensing, v. 51, p. 681-687.

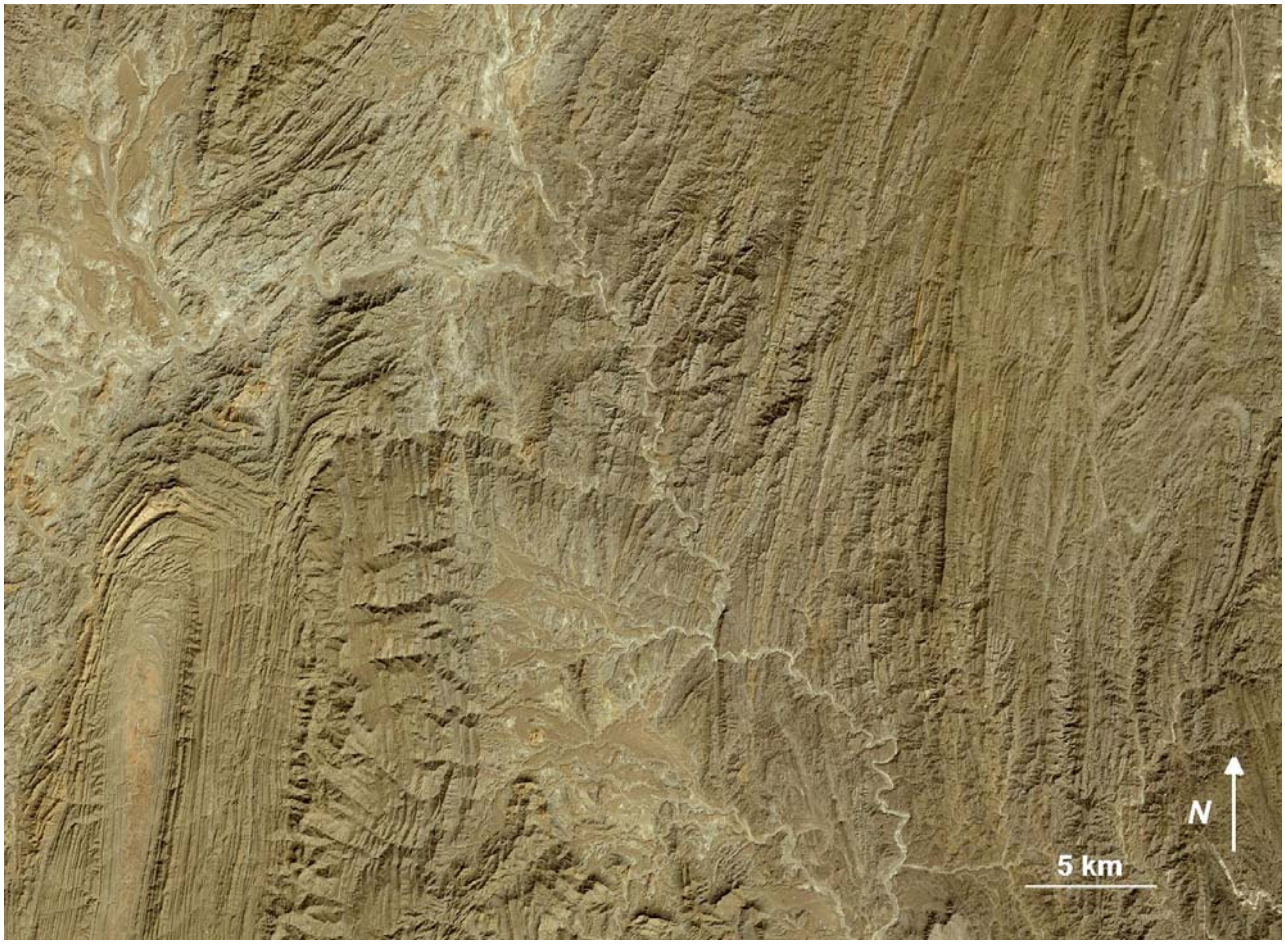

Figure 1. Landsat ETM+ natural-color image of an area in southeastern Afghanistan.

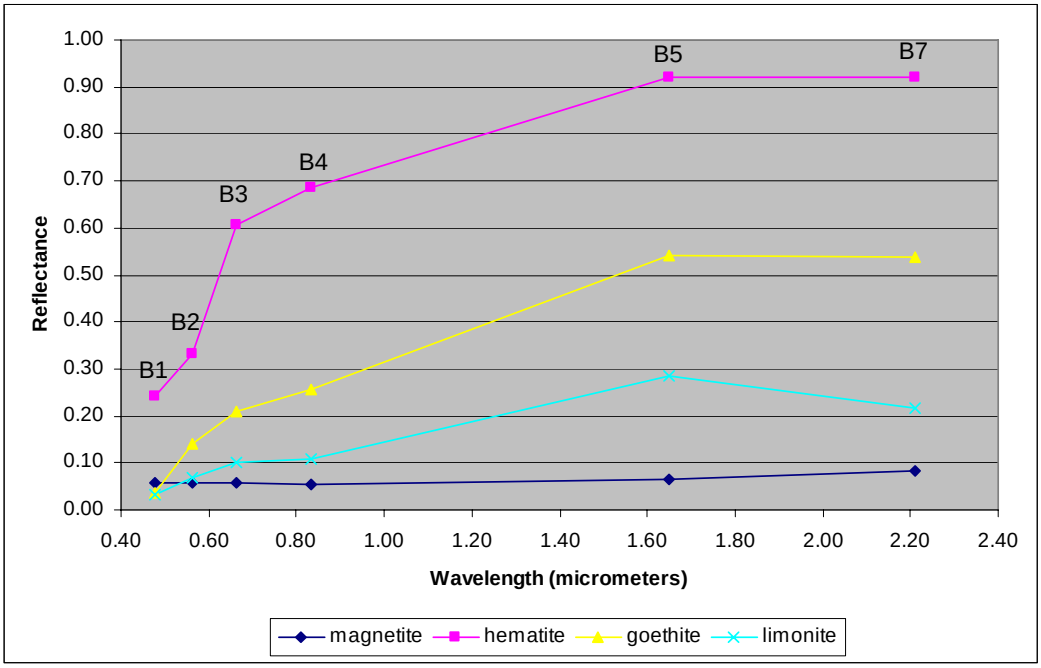

Figure 2. Laboratory reflectance spectra for common iron-oxide minerals (Clark et al., 1993), resampled to the six Landsat ETM+ nonthermal bands, which are designated by "B" numbers.

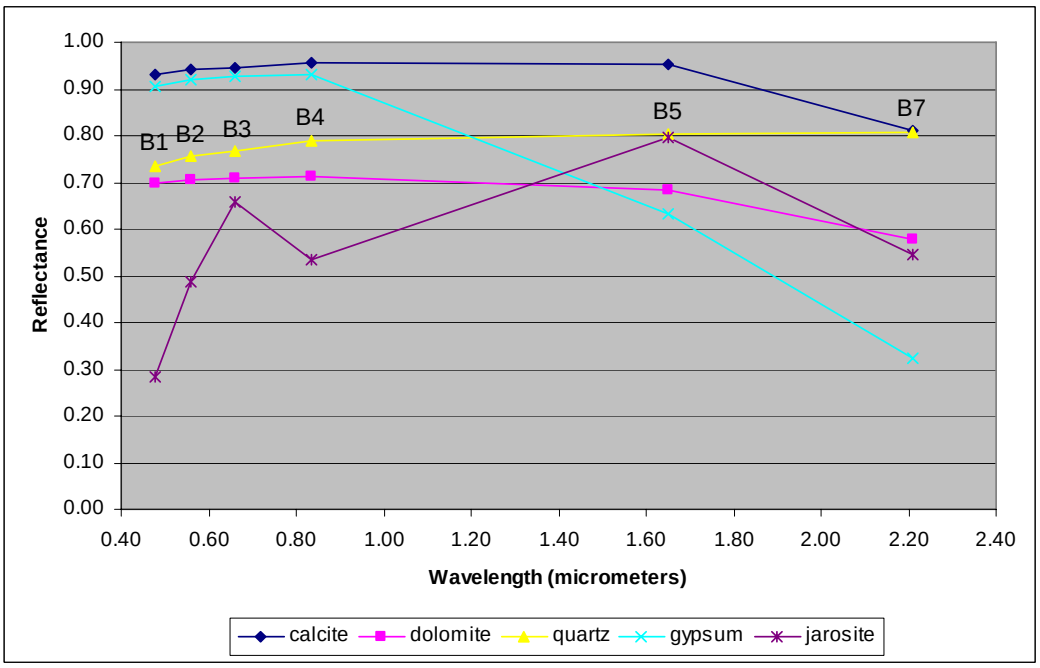

Figure 3. Laboratory reflectance spectra for minerals commonly found in sedimentary rocks and alluvium (Clark et al., 1993), resampled to the six Landsat ETM+ nonthermal bands, which are designated by "B" numbers.

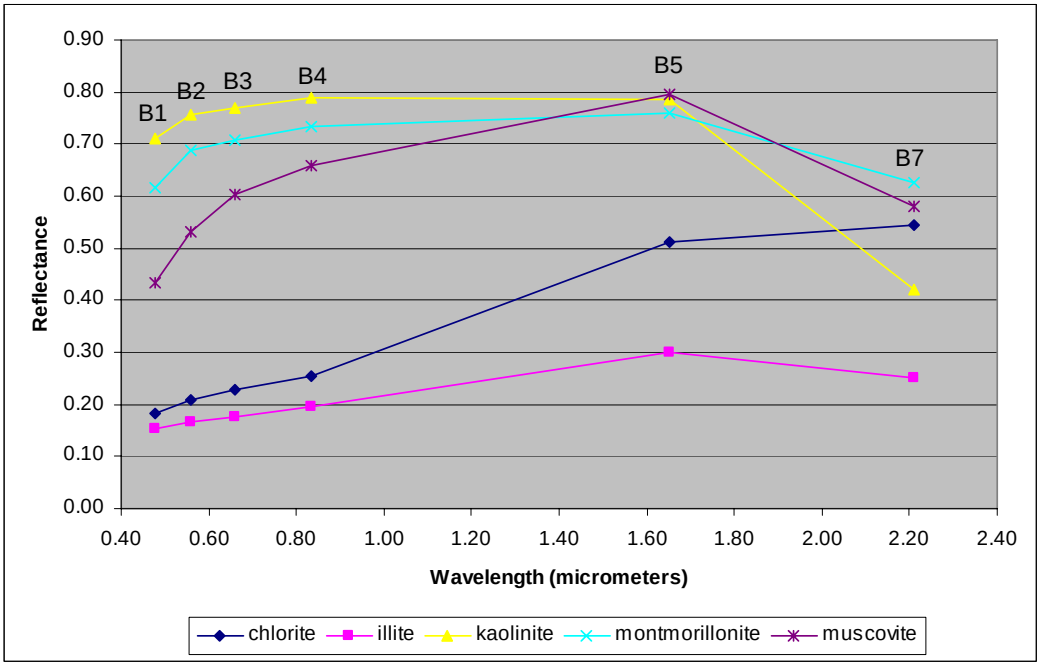

Figure 4. Laboratory reflectance spectra for common phyllosilicate minerals that occur in many different rock types and in alluvium (Clark et al., 1993), resampled to the six Landsat ETM+ nonthermal bands, which are designated by "B" numbers.

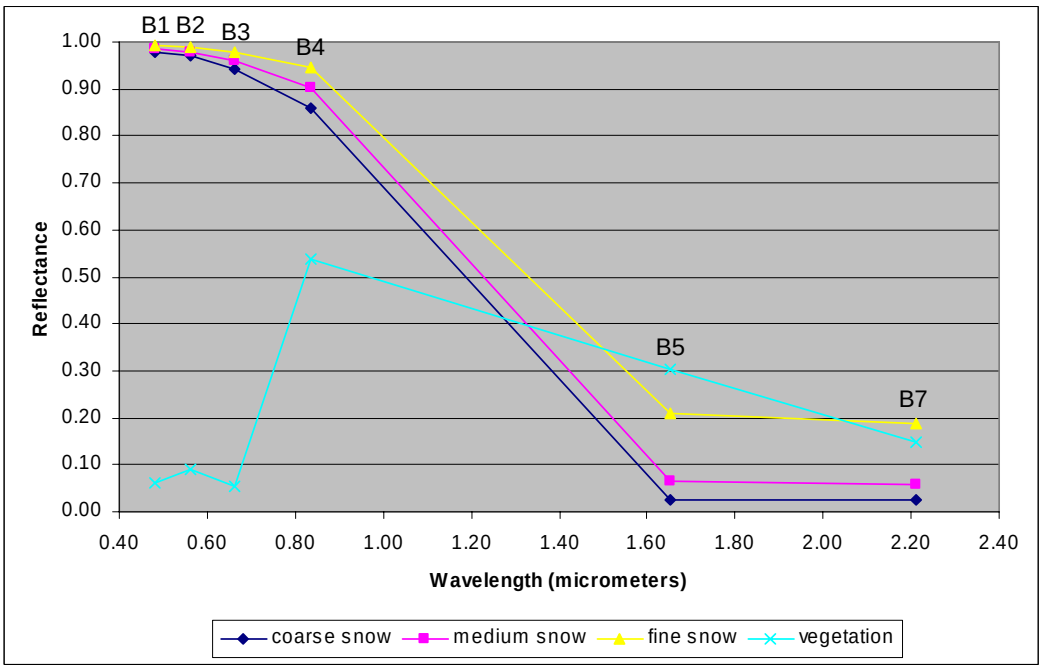

Figure 5. Laboratory reflectance spectra for snow of different grain sizes and for average deciduous vegetation (Clark et al., 1993), resampled to the six Landsat ETM+ nonthermal bands, which are designated by "B" numbers.

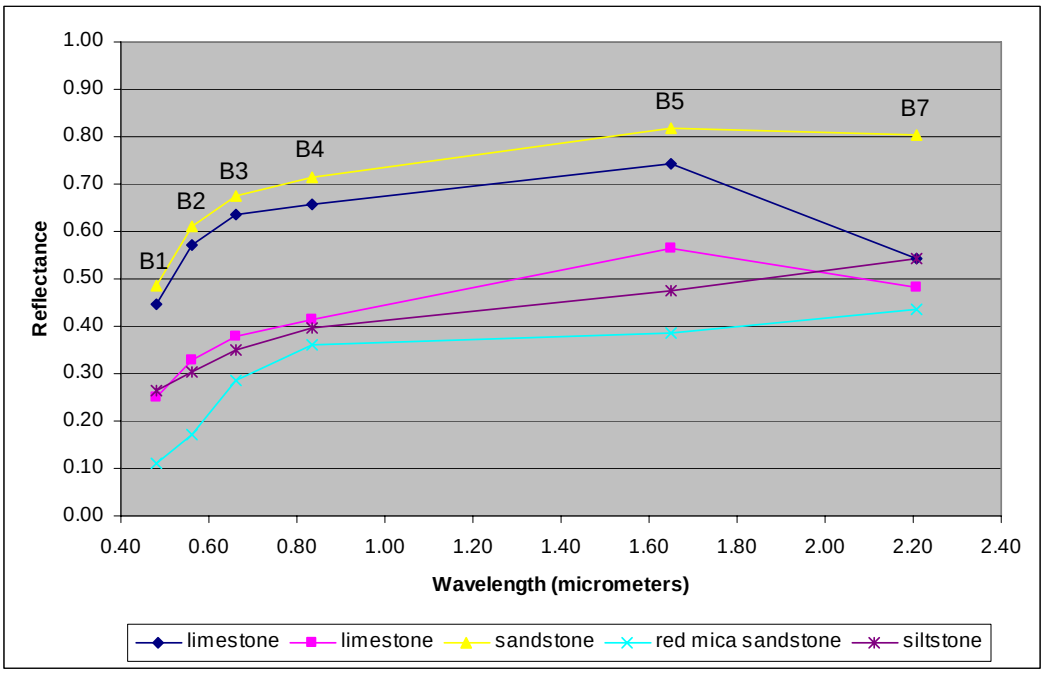

Figure 6. Laboratory reflectance spectra for some common chemical and clastic sedimentary rocks (Clark et al., 1993), resampled to the six Landsat ETM+ nonthermal bands, which are designated by "B" numbers.

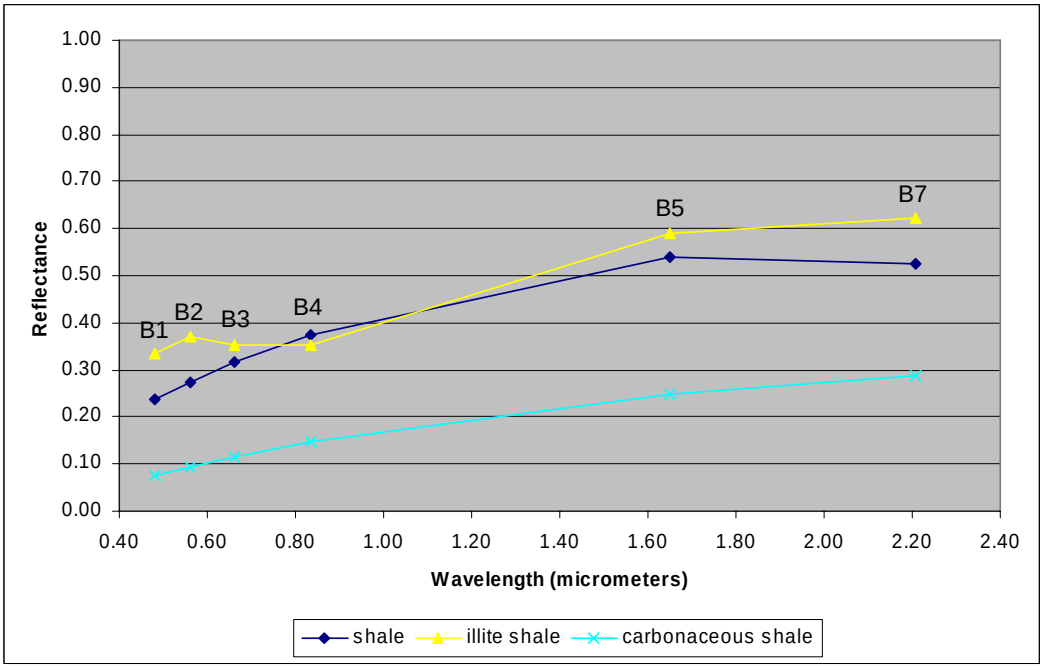

Figure 7. Laboratory reflectance spectra for different shales, which are very fine-grained, fissile rocks (Clark et al., 1993), resampled to the six Landsat ETM+ nonthermal bands, which are designated by "B" numbers.

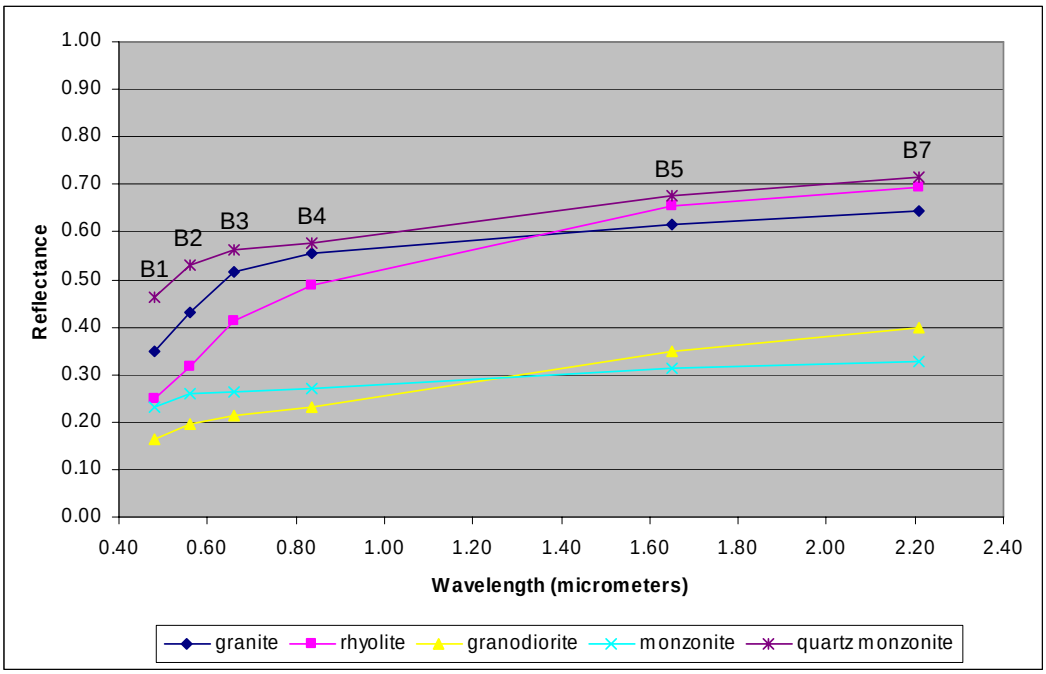

Figure 8. Laboratory reflectance spectra for common siliceous igneous rocks (Clark et al., 1993), resampled to the six Landsat ETM+ nonthermal bands, which are designated by "B" numbers.

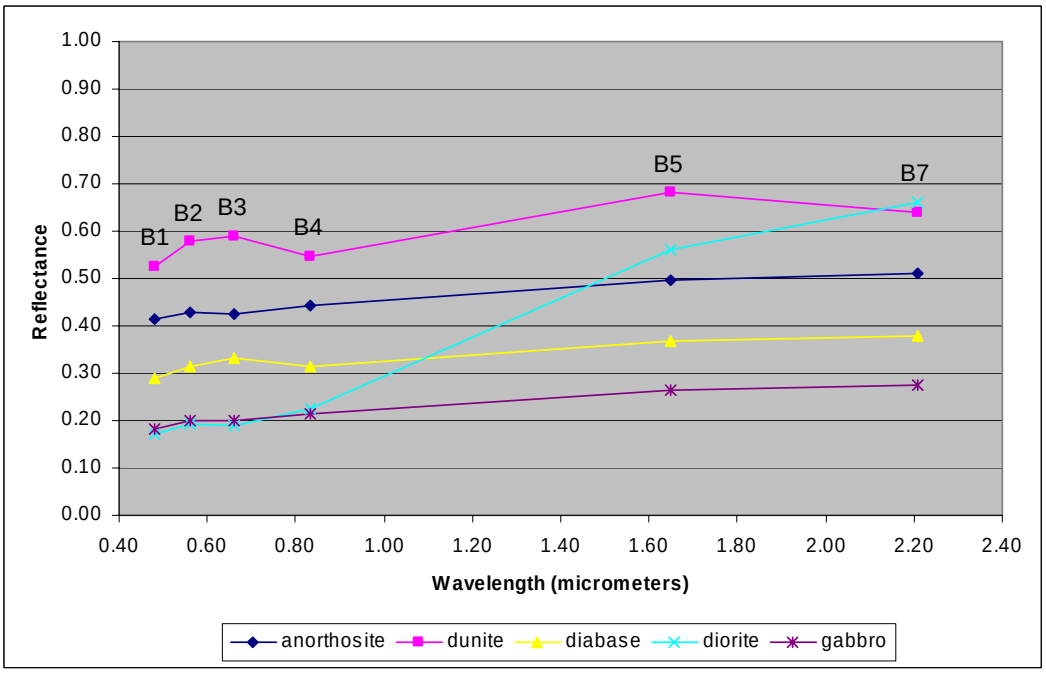

Figure 9. Laboratory reflectance spectra for some common mafic and ultramafic (anorthosite and dunite) igneous rocks (Clark et al., 1993), resampled to the six Landsat ETM+ nonthermal bands, which are designated by "B" numbers.

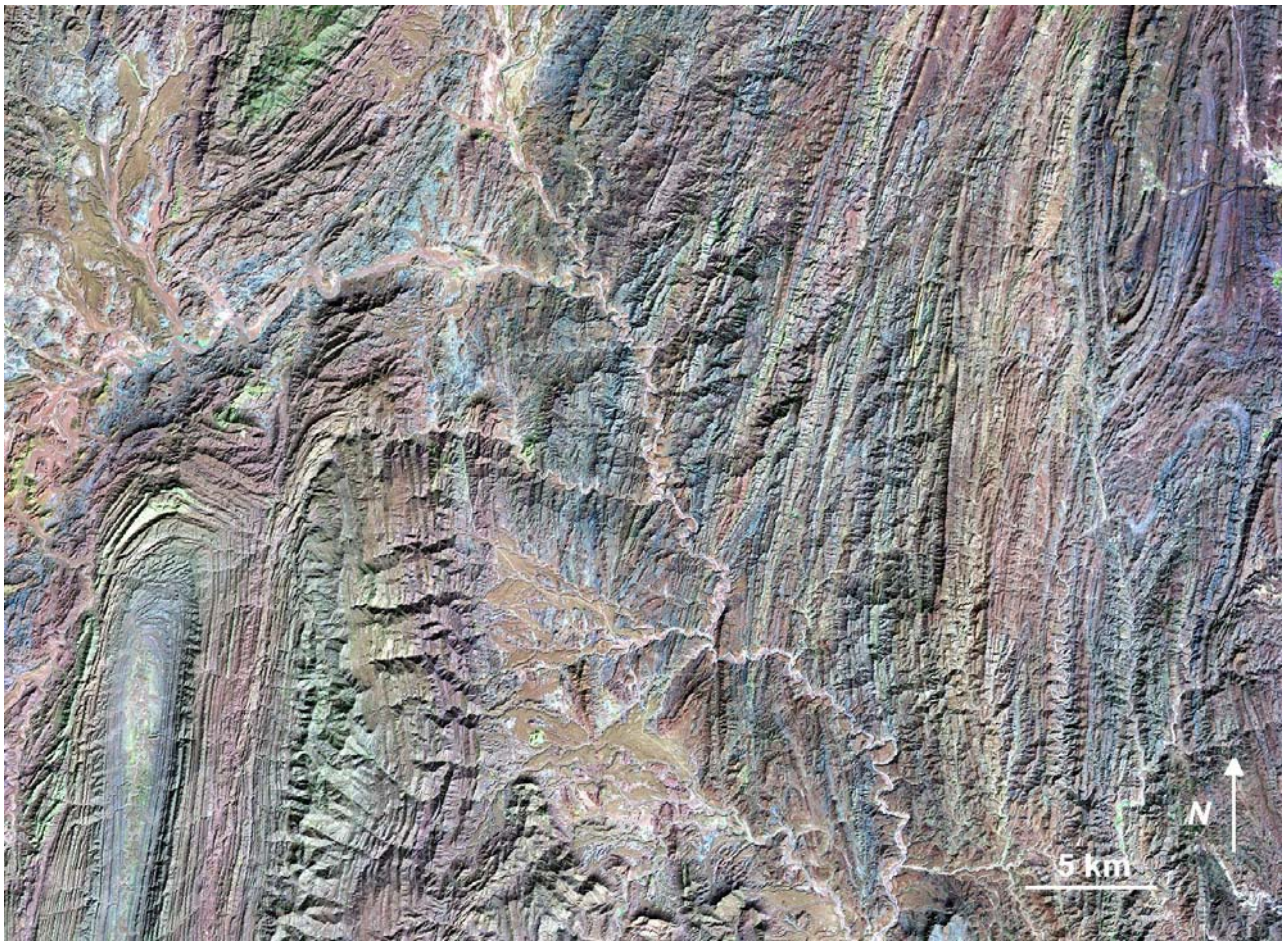

Figure 10. Landsat ETM+ false-color image of same area shown in Figure 1

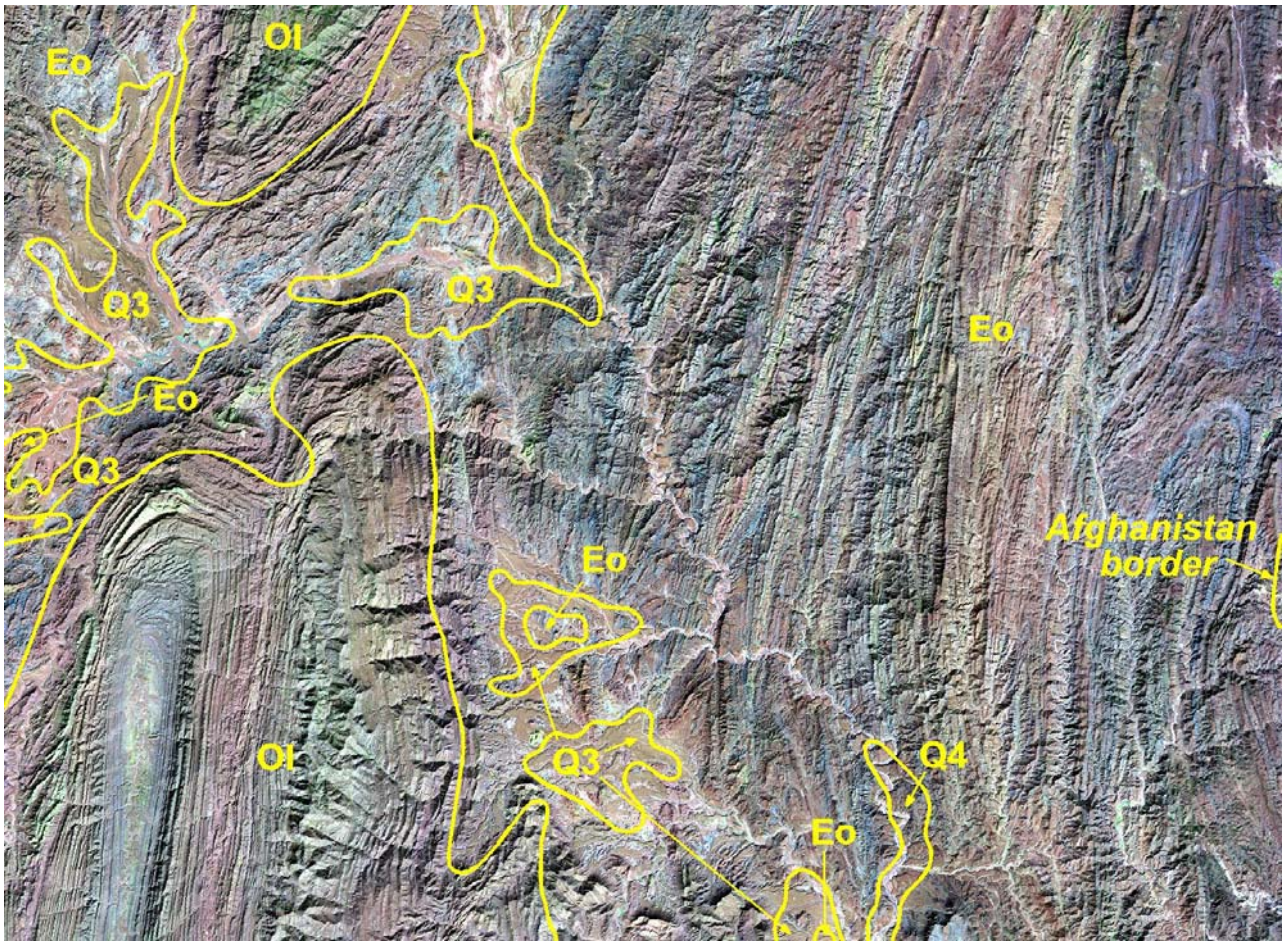

Figure 11. Russian geology (Sborshchikov et al., 1972) superposed on the Landsat ETM+ false-color image in Figure 10.

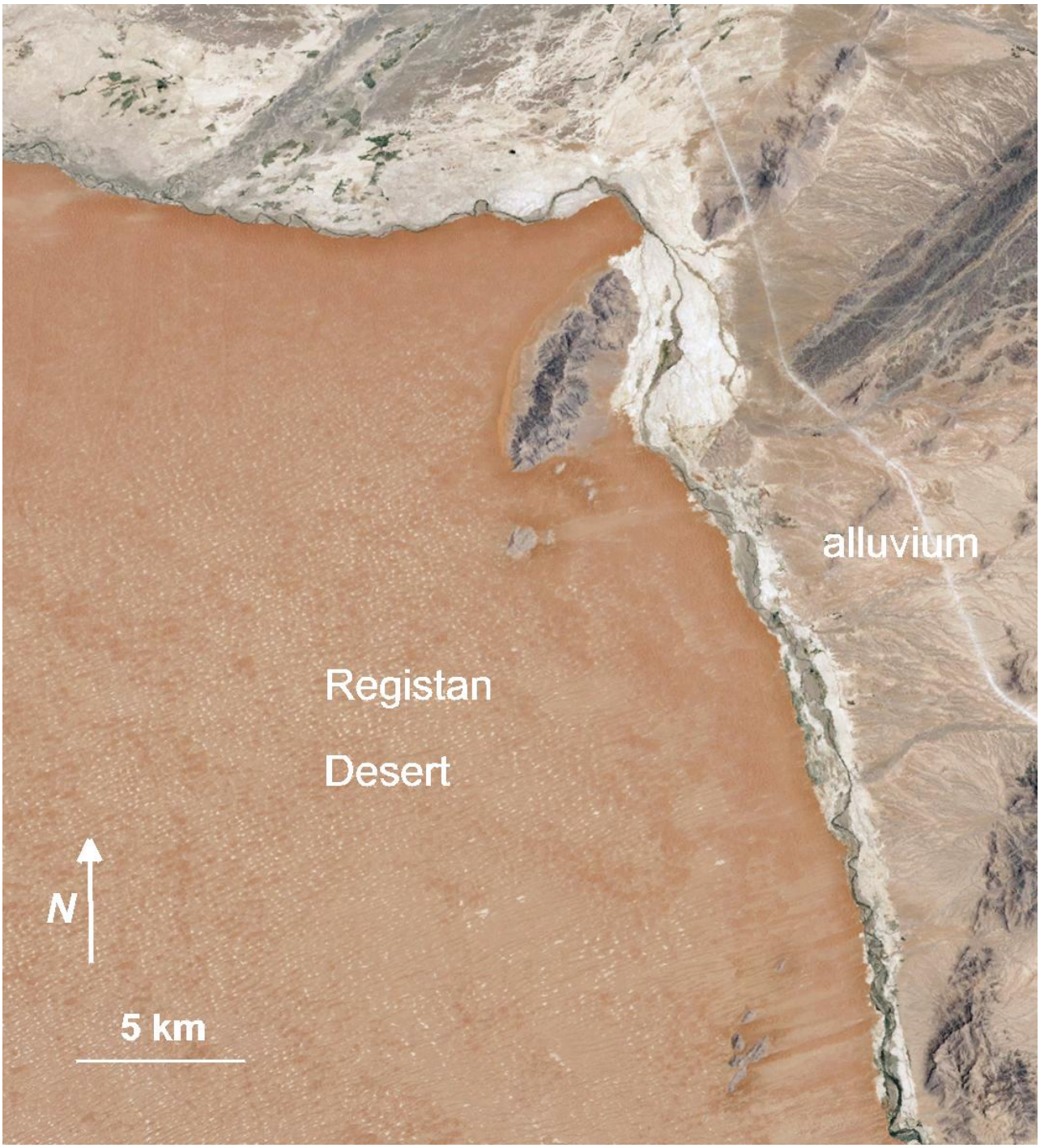

Figure 12. Landsat ETM+ natural-color image of the northeastern border of the Registan Desert where drift sand (orange) meets bright white alluvium along a river valley.

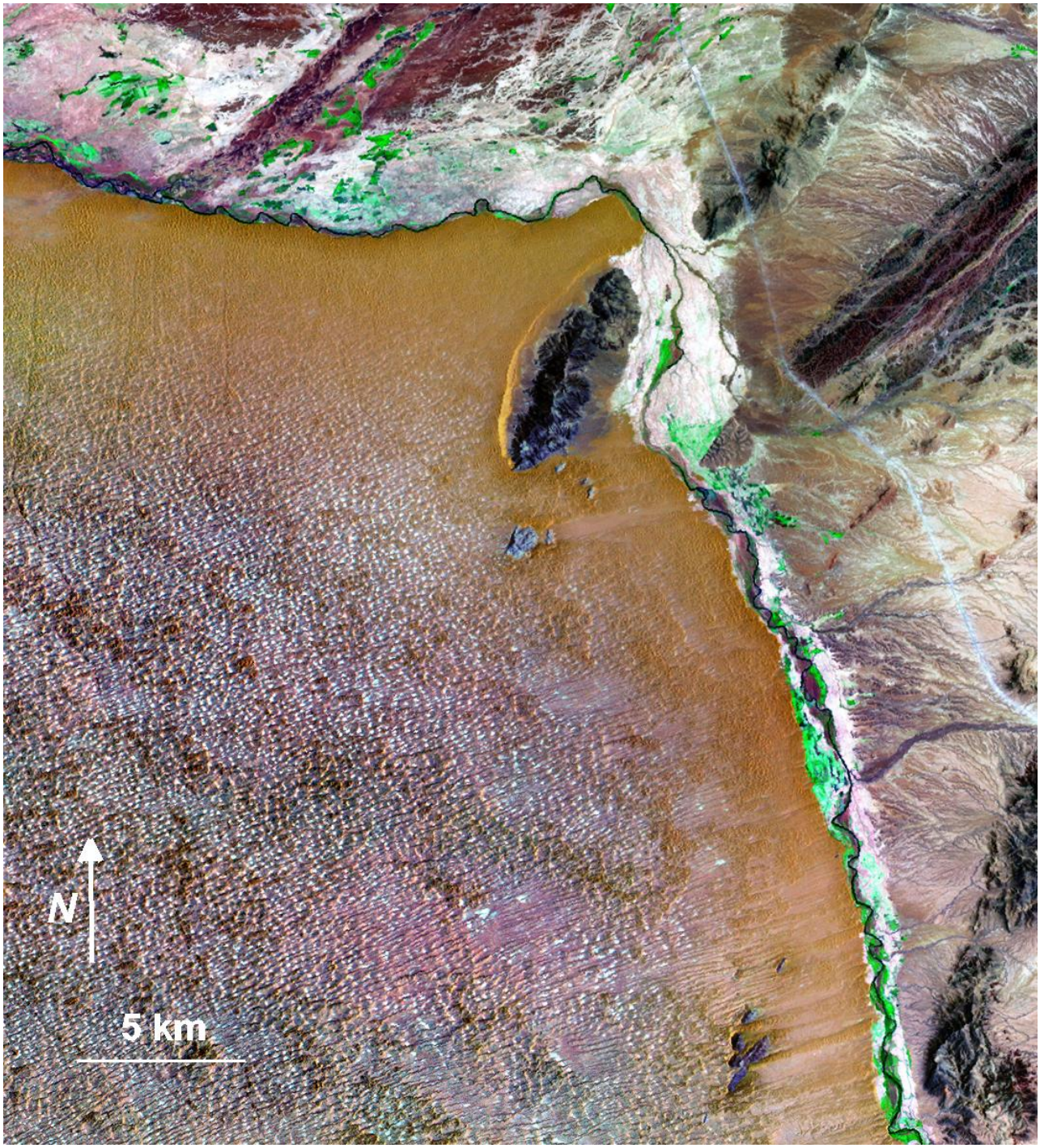

Figure 13. Landsat ETM+ false-color image of area shown in Figure 12 where drift sand (orange) meets alluvium (white and magenta), river (sinuous dark), and vegetation (green).

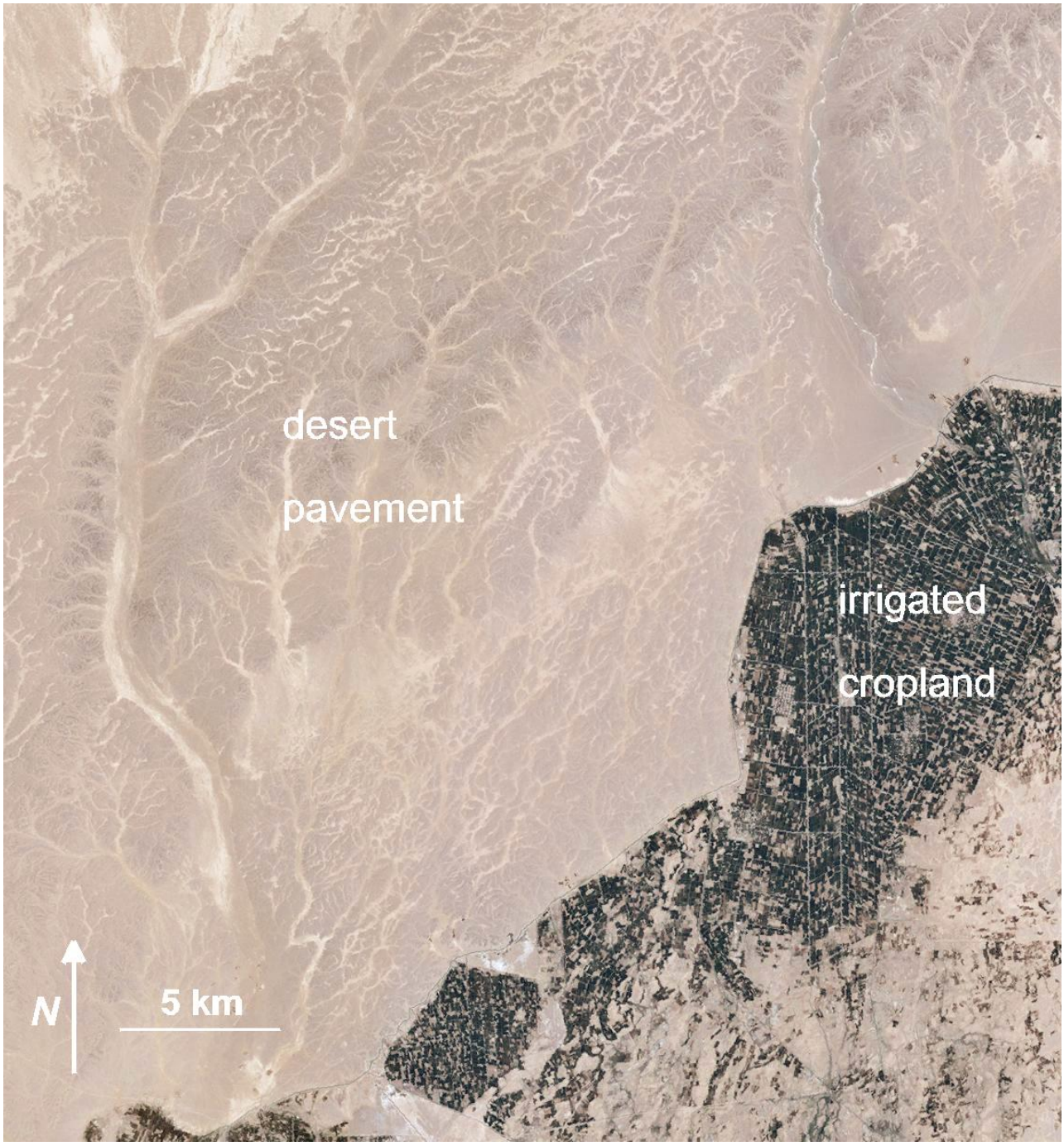

Figure 14. Landsat ETM+ natural-color image of an area north of Registan Desert in southern Afghanistan where irrigated alluvial areas are adjacent to desert pavement.

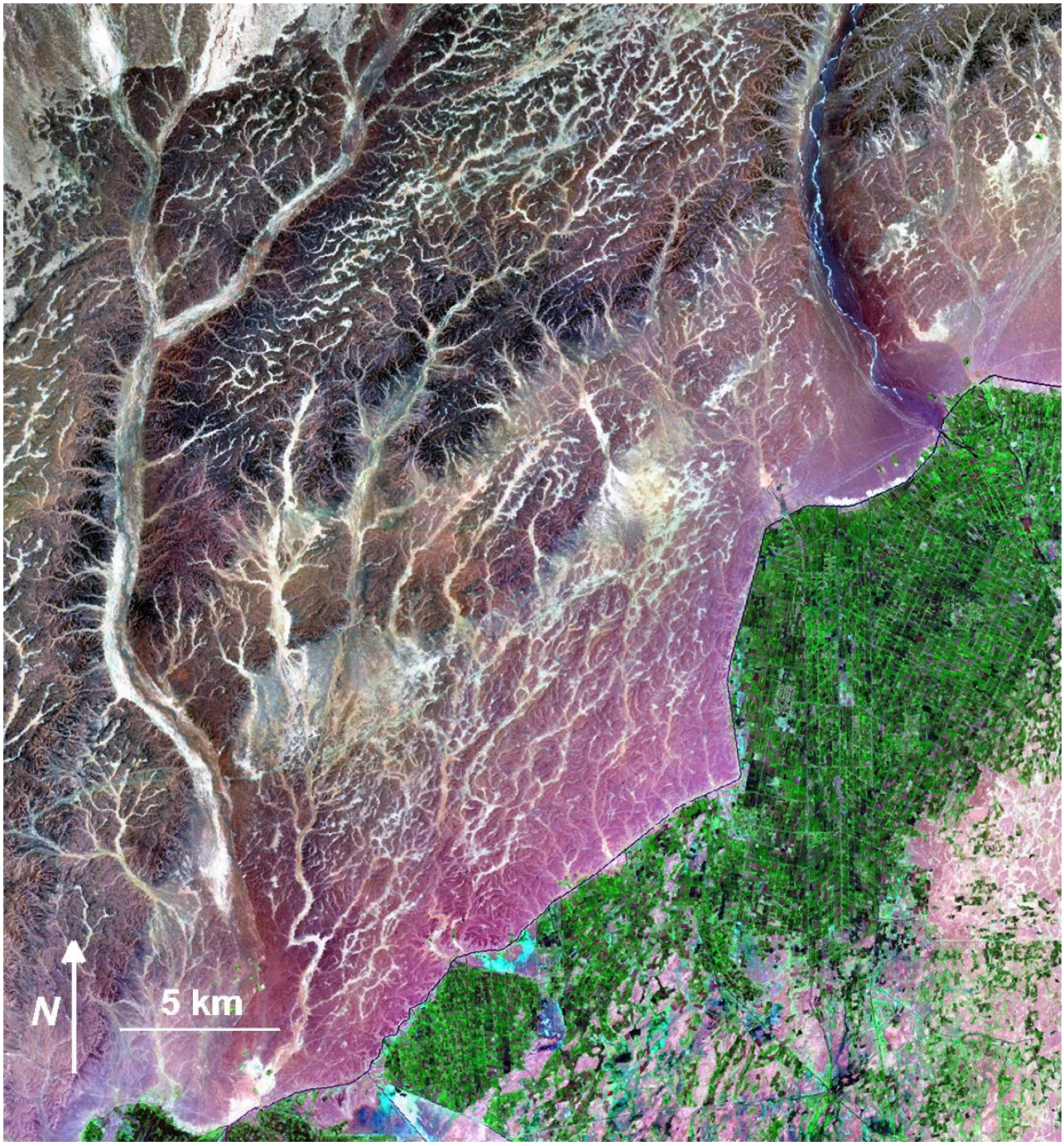

Figure 15. Landsat ETM+ false-color image of area shown in Figure 14 where irrigated alluvial areas (green) are adjacent to desert pavement (dark brown).

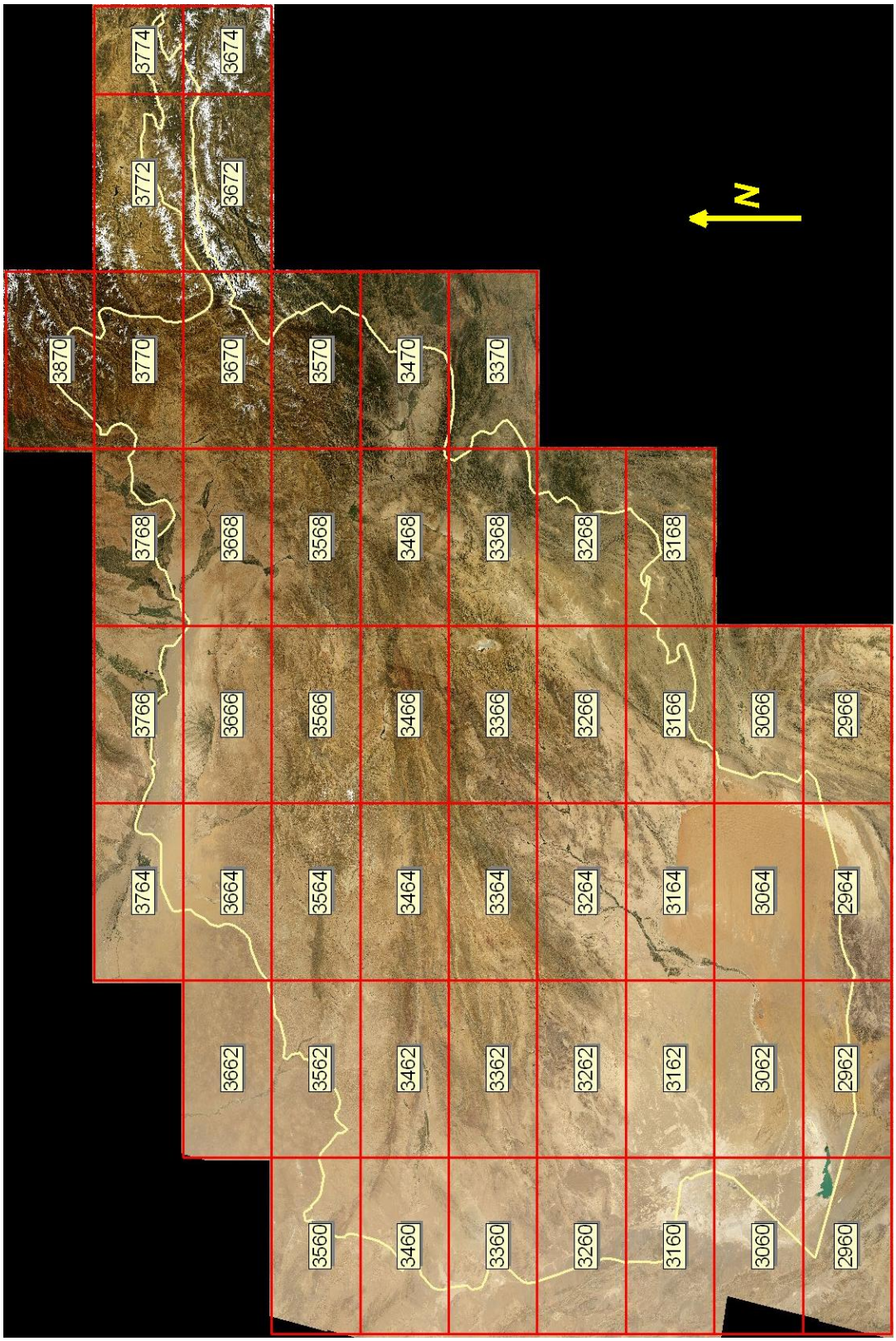

Figure 16. Map tile scheme for the Afghanistan project (on a natural-color image base) with each 1° x 2° map quadrangle designated by its lower left latitude and longitude.